nature physics

ARTICLES

https://doi.org/10.1038/s41567-018-0217-6

Doping the holographic Mott insulator

Tomas Andrade[1], Alexander Krikun[2*], Koenraad Schalm[2] and Jan Zaanen[2]

Mott insulators form because of strong electron repulsions and are at the heart of strongly correlated electron physics. Conventionally these are understood as classical 'traffic jams' of electrons described by a short-ranged entangled product ground state. Exploiting the holographic duality, which maps the physics of densely entangled matter onto gravitational black hole physics, we show how Mott-like insulators can be constructed departing from entangled non-Fermi liquid metallic states, such as the strange metals found in cuprate superconductors. These 'entangled Mott insulators' have traits in common with the 'classical' Mott insulators, such as the formation of a Mott gap in the optical conductivity, super-exchange-like interactions and the formation of 'stripes' upon doping. They also exhibit new properties: the ordering wavevectors are detached from the number of electrons in the unit cell, and the d.c. resistivity diverges algebraically instead of exponentially as a function of temperature. These results may shed light on the mysterious ordering phenomena observed in underdoped cuprates.

The 'hard' Mott insulators realized in stoichiometric transition metal salts[1] are regarded as one of the few entities that are relatively[2] well understood in the arena of strongly correlated electron systems. The principles are given away by Hubbard-type models: in a half-filled state with one electron per unit cell, any charge fluctuation gives rise to an excess local Coulomb energy 'U' and when this becomes much larger than the bandwidth, quite literally a traffic jam of electrons is formed. When the spins form a conventional antiferromagnet, this state can be adiabatically continued to the weak interaction limit using (Hartree–Fock) mean-field theory. There, it turns into a 'BCS-like' commensurate spin density wave[3]. The language of quantum information reveals the key element: Hartree–Fock rests on the assumption that the ground state is a 'semi-classical' short-ranged entangled product state[4]. At strong coupling, the quantized single-electron charges are just localized inside the unit cell. At weak coupling, one has to accommodate Fermi statistics, but it can be shown explicitly that even the Fermi gas is a product state in momentum space[5]. The perfectly nested density wave (weak coupling Mott insulator) then 'inherits' its lack of macroscopic entanglement from the underlying Fermi liquid.

However, matter may also be 'substantially quantum' in the sense of quantum information: the vacuum state may be an irreducible coherent superposition involving an extensive part of the exponentially large many-body Hilbert space. Little is known with certainty given the quantum complexity: an analogue quantum computer is needed to address it with confidence. Indications are accumulating that the strange metals realized in the cuprate high T_c superconductors may be of this kind[6]. Upon lowering the temperature in the under-doped regime, this strange metal becomes unstable towards a myriad of 'intertwined' ordering phenomena that do depend critically on the ionic lattice potential[7,8]. It appears that the characteristic 'pseudogap' scale is small as compared with the ultraviolet cutoff of the strange metal and is thereby reminiscent of the above-mentioned weakly interacting commensurate spin density wave. Nevertheless, it has become increasingly clear that this pseudogap order does not seem explainable in terms of conventional mean-field language[7,9]. Could it be that these ordering phenomena inherit the many-body entanglement of the strange metal? If so, do these submit to general emergence principles of a new kind that can be identified in experiment?

A new mathematical machinery has become available that can address this question to a degree. There is strong evidence that the holographic duality[10] (or anti-de Sitter/conformal field theory (AdS/CFT) correspondence) discovered in string theory describes generic properties of certain classes of such densely entangled quantum matter[6]. In particular, holographic strange metals are emergent quantum critical phases that behave in key regards suggestively similar to the laboratory strange metals (local quantum criticality[11,12], Planckian dissipation[13,14]). Here we will explore what holography has to say about the emergence of 'entangled Mott insulators'.

The results reveal generalities that are intriguing and suggestive towards experiment. On the one hand, the holographic realization of the Mott insulator shows properties similar to the conventional variety. The optical conductivity has similar characteristics to the inter Hubbard band transitions found in hard Mott insulators (Fig. 1e)[15,16] and an analogue of superexchange interaction[17,18] can be identified (Fig. 1f). Upon doping, close analogies of the 'spin stripes'[19–23] are formed. However, this state also reveals unconventional features reflecting its entangled nature. Reminiscent of the charge density wave (CDW) state in cuprates, the periodicity of the charge order that forms upon doping displays commensurate plateaux, staying constant in a range of doping levels. Most intriguingly, holography insists that charge cannot be truly localized as in a conventional Mott insulator. Instead, a reconfigured quantum critical phase emerges at low energies. It is characterized by a d.c. resistivity that increases algebraically instead of exponentially for decreasing temperature, reminiscent of the puzzling slow rise of the resistivity in striped cuprates. The existence of this quantum critical, non-localizable, phase in the low-temperature underdoped region of the phase diagram is a crucial prediction of our study. As we discuss below, this phase presents a unique arena for experimental study of the quantum strongly entangled matter.

Let us now discuss how we arrive at these results. The necessary condition for conventional Mott insulators to form is that the unit cell contains an integer number of electrons. However, in strongly entangled states including the ones described by holography, the information regarding the graininess of the microscopic electron charge is generically washed out. There is, nonetheless, an alternative and truly general definition of a Mott insulator that circumvents the confines of microscopic product states: a Mott insulator

[1]Departament de Física Quàntica i Astrofísica, Institut de Ciències del Cosmos (ICCUB), Universitat de Barcelona, Barcelona, Spain. [2]Institute-Lorentz for Theoretical Physics, Leiden University, Leiden, the Netherlands. *e-mail: krikun@lorentz.leidenuniv.nl

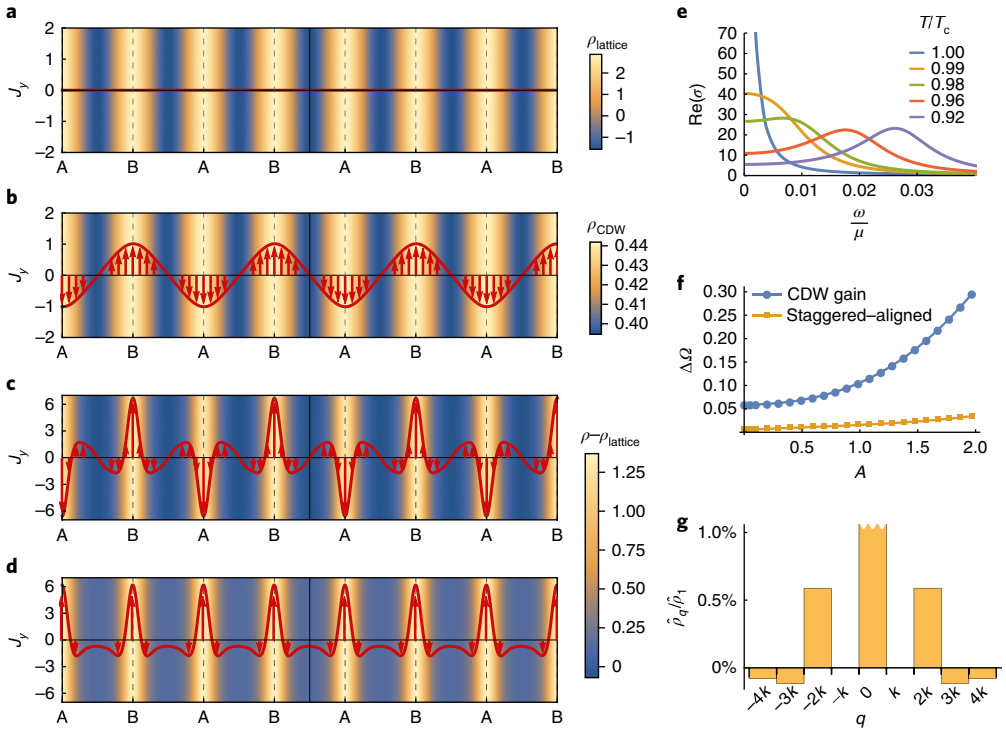

Fig. 1 | Formation of the holographic Mott insulator. a–d, Profiles of the spontaneous currents (arrows) and charge density (colour) in the ionic lattice without spontaneous order (unbroken phase) (**a**), the purely spontaneous intertwined CDW state (**b**), the commensurately locked Mott state (**c**) and the state with aligned currents (**d**). Due to intertwinement of order, this latter state has a different charge density from the Mott state. Note that the total current is zero in both staggered and aligned states. All solutions are at a fixed chemical potential with $T=0.01\mu$, lattice potential strength $A=2$ and θ-coupling $c_1=17$. **e**, Evolution of optical conductivity through the phase transition from the metallic state to the Mott state. A sharp Drude peak is seen in the metallic state that is pinned and broadened after the phase transition ($A=0.7$, $c_1=17$, $T_c\approx0.15\mu$). **f**, Energy scales and superexchange. The grand thermodynamic potential difference between the unbroken phase and the Mott state (blue line) and for the Mott state and the state with aligned currents (yellow line), as a function of the strength of the lattice potential. Clearly, the energy scale of the current ordering lacks behind the one of the charge ordering when the lattice becomes strong. Note that the grand canonical ensemble is required due to the charge difference between the two current configurations ($T=0.01\mu$, $c_1=17$). **g**, Higher harmonics. The difference between the Fourier transform of the charge density $\hat{\rho}_q$ of the aligned (**d**) and staggered (**c**) states. Both spectra are normalized with respect to the lattice periodic mode ($\hat{\rho}_k$). The enhancement of the $2k$ mode is seen for the aligned state, showing that it has twice the number of CDWs per unit cell. The enhancement of the homogeneous component by ~10% in not shown.

is an electron crystal that is commensurately pinned by a periodic background potential. A crystal formed in the Galilean continuum is a perfect metal since it can freely slide—its massless longitudinal phonon mediates the current that is protected by total momentum conservation. This sliding mode will acquire a pinning energy in a commensurate background lattice and this is the general meaning of a Mott gap. In what follows we will rely on this general definition of the Mott state.

This is not a practical way to construct a Mott insulator departing from the electron gas at metallic densities since it lacks a natural tendency to crystallize. Holographic strange metals, on the other hand, are known to have crystallization tendencies, where the most natural form[24] intriguingly involves a most literal form of 'intertwined' order similar to that observed in underdoped cuprates[7,8,25–31]. The AdS/CFT correspondence shows that the properties of quantum matter can be computed in terms of a holographic gravitational 'dual' in a space with one extra dimension[6,10]. Strange metallic states appear to be in one-to-one correspondence to charged black holes in this gravitational system. It was discovered that topological terms in the gravity theory (theta- and Chern–Simons terms in even and odd dimensions) have the effect that the horizon of the black hole becomes unstable towards spatial modulations[32,33] at the 'expense' that the charge modulation is 'intertwined'[34] with parity breaking and the emergence of spontaneous diamagnetic currents.

Here we study this holographic crystallization in the presence of an external periodic potential. This demands advanced numerics to solve the gravitational problem; our 'corrugated black holes' are among the most involved solutions in stationary general relativity. To keep the computations manageable, we focus on simple harmonic background potentials and especially an unidirectional translational symmetry breaking. We consider here specifically the minimal version of such a gravitational theory[33]. The basis is Einstein–Maxwell theory in $3+1$ dimensions with a negative cosmological constant, describing the simplest holographic strange metal in $2+1$ dimensions. The crucial extra ingredient is the ϑ-term that couples the Maxwell field A_μ with field strength $F_{\mu\nu}$ to a dynamical pseudoscalar field ψ, such that the action becomes

$$S = \int \mathrm{d}^4x\sqrt{-g}\left(R-2\Lambda-\frac{1}{2}(\partial\psi)^2-\frac{\tau(\psi)}{4}F^2-W(\psi)\right) -\frac{1}{2}\int\vartheta(\psi)F\wedge F \quad (1)$$

It is worth noting here that despite the fact that the 'bare' ϑ-term is parity and time-reversal odd, by coupling it to the dynamical pseudoscalar, we keep the P- and T-symmetry of the action intact. The qualitative features we reveal depend only mildly on the precise form of the functions $\tau(\psi)$, $W(\psi)$ and $\vartheta(\psi)$ (see Methods). The solu-

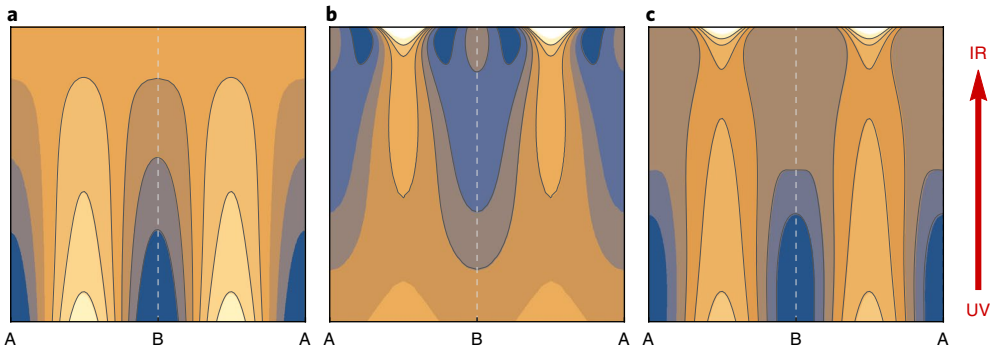

Fig. 2 | Holographic renormalization group pattern. a–c, The profiles of the electric field strength $\partial_z A_t$ (see equation (9) in the Methods) in the gravitational theory encoding the renormalization group flow from the ultraviolet (UV, bottom) to the infrared (IR, top) of the pure lattice that is sourced in the ultraviolet and decreases to irrelevancy in the infrared (**a**), the spontaneous CDW that emerges in the infrared, but does not have sources in the ultraviolet (**b**) and the lock-in that forms the Mott state (**c**). The CDW locks to the lattice at intermediate scales and introduces the relevant explicit translation symmetry breaking in the infrared, giving rise to the insulating state. The values shown in coulour are independently scaled to unit interval revealing the field strength pattern in each case.

tion to the equations of motion will asymptote to AdS space, on the (conformal) boundary on which the dual theory lives. At finite density and temperature, a charged (Reissner–Nordström) black hole is present in the deep interior, which famously translates to a locally quantum critical strange metal[6,12] (see Methods for the dictionary entries). As the temperature is lowered, the ϑ-term causes the spatially modulated instability of the horizon that breaks translations spontaneously. Here we choose the simplest version, corresponding to a unidirectional symmetry breaking in the 'x' direction (see refs [34,35] for a 'full' 2D crystallization). This is driven by the condensation of the pseudoscalar ψ representing a spontaneous breaking of parity on the boundary. The structure of the ϑ-term means that this is accompanied by condensation of the Maxwell field strength that translates into the formation of spontaneous currents running in the y direction with a concomitant charge density wave (CDW). A reliable, consistent result is obtained only if one solves the full equations of motion in the gravitational theory, and this includes the change in geometry due to back-reaction. Given the inhomogeneous nature of the bulk space time, this involves a considerable numerical general relativity effort since the Einstein equations represent a system of nonlinear partial differential equations (see Methods). The result is represented in Fig. 1b.

One can also introduce a background periodic potential that breaks translational symmetry explicitly by representing the ion lattice in terms of a spatially modulated chemical potential in the field theory[36–42]. It is straightforward to incorporate complicated forms of such 'pseudo potentials', but we will focus again on the simplest choice in the form of a unidirectional single harmonic potential with wavevector k and relative amplitude A: $\mu(x)=\mu_0(1+A\cos(kx))$ (Fig. 1a). As we show below, even this simplified unidirectional model possesses the key features that we are after and which will remain in a more realistic two-dimensional set-up.

Combining these two allows us to study spontaneous holographic crystallization in the presence of a background lattice. The crystal tends to form with a preferred intrinsic wavelength p_0 set by the ϑ-coupling and the scale of the mean charge density. In the presence of a periodic potential characterized by wavevector k, one anticipates the physics of incommensurate systems, which were studied thoroughly in classical matter[43,44]. As found in an earlier study[45], when these periodicities are sufficiently close together, one expects a 'commensurate lock-in' effect to provide an additional stability to the state where the period of the spontaneous crystal equals that of the lattice. This lowest-order commensurate state is the holographic incarnation of the Mott insulator (Fig. 1c), according to the above-mentioned general definition.

It is instructive to consider the features of this state, starting from the optical conductivity. In the absence of the periodic potential, one finds a 'diamagnetic' delta function peak at zero frequency at all temperatures. The reason is that every finite density system is a perfect metal in the spatial continuum limit since total momentum is conserved. The formation of a crystal at T_c spontaneously breaks translational invariance, and a longitudinal phonon emerges—the sliding mode—which mediates a perfect current. When we now switch on an explicit commensurate background potential, this mode will acquire a mass since the crystal gets pinned and it can no longer freely slide. This reveals itself in the optical conductivity (Fig. 1e). As the crystal forms below T_c, the metallic Drude peak rapidly moves off to finite frequency corresponding to the pinning of the sliding mode. The mode itself broadens first due to increased translational symmetry breaking from the crystal. The resulting optical conductivity at $T<T_c$ is similar to that of a hard Mott insulator with a broadening due to Hubbard interband transitions.

From Fig. 1c, one infers that the background lattice enhances the spontaneous order. Visually, one notices that the currents are generically enhanced in the regions where the spontaneous CDW has a maximum and the current density is effectively localized in these regions. This charge localization together with the alternating pattern of these currents immediately calls to mind the hard antiferromagnetic Mott insulator with staggered spins.

This suggests that other current patterns also exist. Indeed, metastable solutions (local minima in the grand thermodynamic potential Ω) exist where the currents are aligned (Fig. 1d). In the presence of a large lattice potential, the energy difference between these two configurations is much smaller than the energy difference between the CDW ordered and the uncrystallized state (Fig. 1f). This implies that current–current dynamics is governed by a different scale from charge dynamics. It is in analogy with the spin-charge separation in conventional Mott insulators, where below the Mott transition the spin order is governed by effective 'super exchange' interactions that are much smaller than the scale associated with the Mott insulator itself. Keeping this analogy in mind, one anticipates the effect the thermal fluctuations will have on the system. For strong lattice potentials, one first encounters the onset of the CDW order at the transition temperature. Only at lower temperature will the additional staggered current symmetry breaking occur, since the latter will remain thermally disordered at temperatures larger than the current–current 'exchange' parameter. A full thermodynamic treatment of the holographic model will exhibit this physics.

A highlight of holography is that the extra dimension of the gravitational theory can be interpreted as the 'scaling direction' of

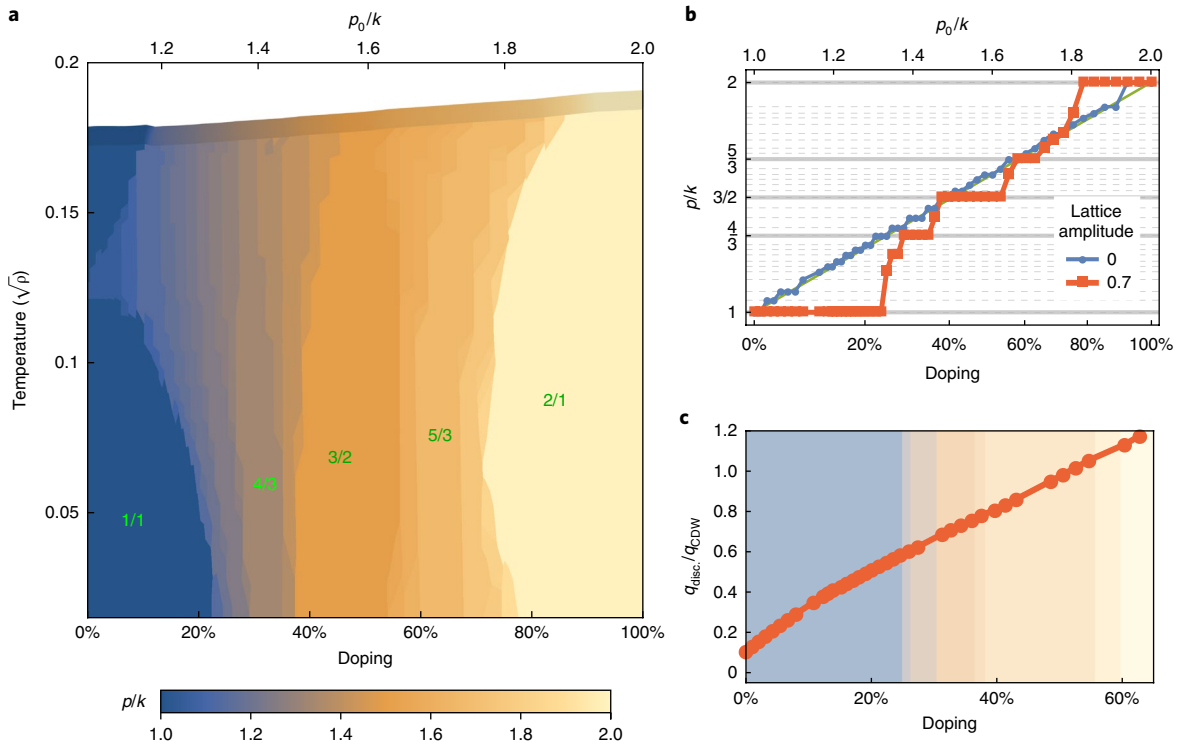

Fig. 3 | Doped states. a, Doping the holographic Mott insulator. The colour shows the thermodynamically preferred commensurate fraction as a function of doping and temperature. The regions of stability of the leading 1/1, 2/1 and, as temperature is lowered, higher commensurate points (3/2, 4/3, 5/3) are seen. The shaded line at the top shows the result of perturbative analysis of instabilities (see Methods). Data are taken for $A=0.7$, $c_1=17$. **b**, The commensurate plateaux as seen on the fixed temperature cut ($T\approx 0.01\sqrt{\rho}$) of the phase diagram. Importantly, the commensurate states stay stable for a range of the charge density values. Higher commensurate points 3/2 and 4/3 correspond to $2a$ and $3a$ discommensuration lattices, respectively (a—the lattice constant). p_0/k shows the relation between spontaneous momentum of the free CDW versus the momentum of the lattice. The blue points represent the result in the absence of commensurate lock-in: when the amplitude of the lattice potential vanishes, the preferred momentum of the structure equals the spontaneous one. The gridlines show the mesh of numerical study, where different saddle points were obtained. **c**, Charge of a discommensuration as a function of doping (red line), measured in units of CDW charge density integrated over a unit cell (see equation (20)). The charge is obtained by considering an isolated discommensuration (one over 19 unit cells) and subtracting the contribution of the parent Mott state. The charge changes continuously as the doping is increased. The shading shows the preferred commensurate fraction as in **a**; no signs of plateaux are seen in the charge of discommensuration.

the renormalization group of the dual field theory with the ultraviolet fixed point located on the boundary of AdS. This yields a vivid renormalization group view of the way that the holographic Mott insulator is formed and reveals deep analogies with the conventional variety. The pure holographic ionic lattice potential is always irrelevant in the infrared[40]. This is illustrated in Fig. 2a: the electric field sourced by the external potential falls off moving from the boundary to the deep interior. Therefore, the corresponding state is a metal, similarly to the conventional Mott insulator, which would be metallic if one would consider only the effects of lattice potential on the non-interacting electrons. However, the spontaneous crystal displays precisely the opposite flow: it is relevant in the infrared without having any sources in the ultraviolet (Fig. 2b). Without the explicit lattice though, it has a sliding mode and zero resistance. One can now read off the commensurate pinning mechanism from the 'scaling diagram' (Fig. 2c): this pinning occurs at intermediate energy scales. One sees that 'halfway' the radial direction the (decreasing) field profile sourced by external potential starts to overlap with the (increasing) field strength of the spontaneous crystal. This overlap locks the infrared-relevant translation symmetry breaking by the crystal to the explicit ultraviolet lattice rendering the whole system insulating. In a similar fashion, the conventional Mott insulator forms when the otherwise metallic half-filled state gets insulating due to the effect of the interactions.

The important question with reference to the cuprates is: what happens when these holographic Mott insulators are doped? Above, we tuned the wavevectors of the explicit lattice and spontaneous crystal to be the same. Altering the charge density ρ by adding more charge, the crystal will tend to form at a different intrinsic wavevector $p_0\sim\rho$ but the external lattice potential may force it to acquire some other wavevector p, commensurate with the lattice momentum k. Mismatch between p and p_0 will, however, cost potential energy due to the elastic response of the crystal, so the resulting value of p is determined dynamically by these two competing mechanisms. This is a motive familiar from the study of classical incommensurate systems[44,46] and one anticipates that generically this will promote values of $\frac{p}{k}$, which are the rationals of small coprime integers: these are the higher-order commensurate points. The states labelled by the different fractions $\frac{p}{k}$ form a set of the local minima in the thermodynamic potential Ω and the true ground state corresponds to the one with minimal Ω. We performed extensive numerical computations spanning a large parameter space to identify these saddle points.

The lowest-order commensurate state $p/k=1/1$ is obviously the Mott insulator we just discussed in detail. In analogy with the conventional picture of adding microscopic charges per unit cell, we prescribe the doping level as the excess charge per lattice period compared to the Mott insulating state. We normalize by assigning doping level 100% to the $p/k=2/1$ state, which has exactly one

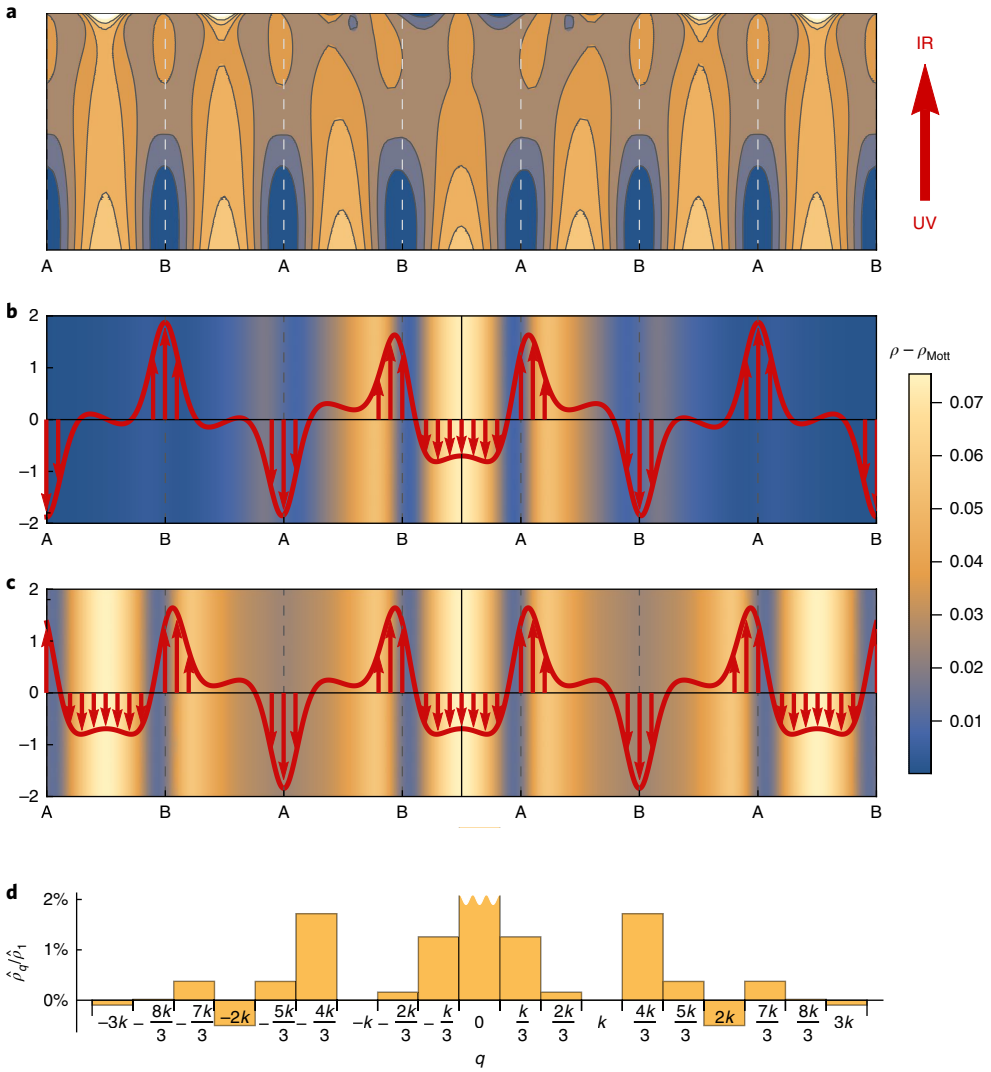

Fig. 4 | Discommensurations. a, Renormalization group structure of an isolated discommensuration (the same notation as on Fig. 2) The ultraviolet lattice locks in the infrared structure everywhere outside the core of a discommensuration. In the core, the 'dislocation' is seen in the electric field, accounting for an excess period of the spontaneous structure in the infrared. **b**, Currents (arrows) and charge density (colour) for an isolated discommensuration. The domain wall in the staggered current (defined using A and B sublattices) is clearly seen as well as excess charge in the core of a discommensuration. **c**, Same data for higher commensurate state with $p/k = 4/3$. The state displays superstructure with a period of 3 unit cells—3a discommensuration lattice. The charge profile is normalized with respect to the corresponding Mott state with $A = 0.7$, $T = 0.01\mu$. **d**, Spectrum of discommensuration lattice. The difference between the Fourier modes of the lattice and the parent Mott insulator. Both spectra are normalized with respect to the lattice periodic mode $\hat{q}_k$. The fractional Fourier modes are clearly enhanced in the discommensuration lattice state. The homogeneous mode reaches ~11% and is not shown.

additional period of spontaneous CDW per unit cell (see Methods). In practice, adding excess charge to the system is accomplished by adjusting the chemical potential, while keeping the lattice wavevector fixed. The result is summarized in Fig. 3a. The crucial feature is that, due to the lock-in, some commensurate points stay stable for a range of dopings, displaying a 'Devil's staircase'-like behaviour familiar from classical incommensurate systems. We shall return to this shortly.

Let us first discuss the structure of these higher-order commensurate states as formed at low temperatures in sufficiently strong background potentials. The periodicity mismatch (the deviation of p/k from 1/1) is concentrated in localized solitonic textures, see Fig. 4b—the discommensurations (see also Methods). This is not completely surprising since discommensurations are rather ubiquitous when dealing with incommensurate systems. It is entertaining to observe how the discommensurations follow the renormalization group in the extra dimension of the gravity system (Fig. 4a). The ultraviolet lattice almost everywhere locks in the infrared CDW, except at the discommensuration core where a curious dislocation is formed in the electrical flux in the radial direction of the gravitational theory.

The noteworthy aspect is that there is additional structure: these discommensurations are, at the same time, domain walls in the staggered current order (Fig. 4b). Considering the current order as being analogous to the antiferromagnetic spin systems found in the standard (doped) Mott insulators, these are just like the famous 'stripes' observed in the La_2CuO_4 (214) family of high-T_c superconductors[20] and in other doped Mott insulators[21]. In the cuprate stripes, the doped charge accumulates at the spin-pattern domain walls and the same is happening here (Fig. 4b). These stripes were actually discovered theoretically on the basis of Hartree–Fock calculations well before the experimental observation[19]. The mean-field stripes have a product state nature that is revealed by the rule that they

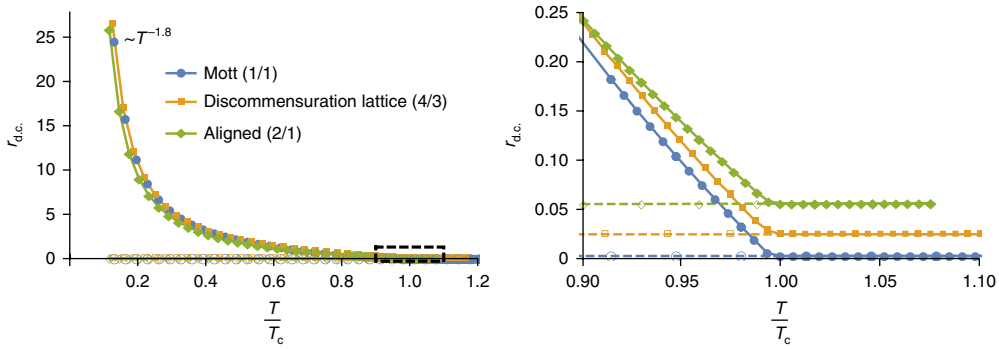

Fig. 5 | The holographic Mott insulator's d.c. resistivity. Left panel: different commensurate states share similar behaviour, revealing power-law scaling at low temperature. This signals the presence of quantum critical degrees of freedom, which remain ungapped. Right panel: at the critical point, no abrupt change of resistivity is seen, suggesting a metal–insulator crossover. The dashed lines show resistivity in the unbroken state without CDW order, which is metallic. Temperature is scaled with respect to the corresponding critical temperature of a given state (see, for example, Fig. 3a).

have a preferred density (typically, one hole per domain wall unit cell). This is crucially different here: the 'holographic stripes' have no preferred charge density. In Fig. 3b, we highlight that the higher-order commensurate plateaux are in fact stable across a range of dopings. This has the implication that the charge density inside the 'stripes' continuously varies over a considerable range (Fig. 3c). It is a natural outcome of the absence of localized quantized charge in this entangled matter. This observation is directly relevant to experiment, which has proved difficult to explain in terms of the conventional 'product state' CDW. In most cuprates, it appears that the periodicity of the charge order locks locally at 4 lattice constants in the large doping range[7–9,47] (the exception is 214 stripes, which do show a sense of preferred charge density in a limited doping range). Our finding is similar to the result obtained recently in the context of numerical approaches to the doped Hubbard model[22,23]. This revealed that stripes are ubiquitous, with a similar surprise that these lack a preferred charge density. These heavy numerical methods wire in entanglement, the same generic motive that is hard-wired in holography. The locked-in periodicity of stripes can therefore be seen as another compelling indication that strong entanglement underlies cuprate strange metals.

Let us now turn to the real surprise revealed by holography: the transport in a holographic Mott insulator is not governed by an activation energy, but instead by an algebraic divergence of the resistivity at zero temperature. In Fig. 5, we show the results for a variety of cases including the 1/1 'Mott insulator'. In all cases at temperatures well below T_c the resistivity diverges algebraically, approximately as $r_{d.c.} \sim T^{-1.8}$. The value of the exponent is not universal, but instead model and state dependent. However, the algebraic fall-off is a generic feature.

This calls to mind a long-standing experimental puzzle that one finds in underdoped cuprates. There is a slow, 'logarithmic'-like, increase of the resistivity setting in at rather high temperatures, seemingly related to the onset of spin-stripe charge order[48,49]. Conventional explanations such as Anderson localization fail to explain this behaviour. However, such a slow rise of the resistivity can be regarded as a universal feature of the holographic Mott state. This universality is hard-wired in the bulk gravity. When the holographic order sets in, the near-horizon black hole geometry that codes for the low-energy physics reconfigures, but does not disappear. This in turn invariably codes for states on the boundary that behave like quantum critical phases with special scaling properties. Our holographic Mott state is a perfect theatre to study this phenomenon. The Drude-like contribution that is governed by momentum conservation is gapped out (see Fig. 1e) and the transport characterized by an 'unparticle' power law is left behind (Fig. 5a). Apparently, this corresponds with a strongly entangled form of matter, inherited from the strange metal, that is not localizable[50]. It is worth stressing here that the unparticle nature of this state invalidates any kind of quasiparticles as mediators of transport. Therefore, the features of resistivity are in principle disconnected from the shape of dispersion relation of either fermionic or bosonic excitations in the system.

This begs the question of whether such matter is realized in the underdoped 'striped' cuprates, revealing itself by the scaling regime in the resistivity at low temperature? The emergence of such scaling from strongly entangled matter is well charted in holography[51–54]. It predicts that many physical properties should give in to algebraic scaling laws, with the exponents that are typically different from those of the high temperature strange metallic phase. This includes thermodynamics (specific heat), thermal transport and magnetotransport, but also optical conductivity at low frequency. We challenge the experimental community to revisit this regime with high precision measurements to find out whether the signatures of strongly entangled matter are realized in cuprates.

In summary, we have identified the holographic analogue of Mott insulators that has crucial phenomenological features in common with the conventional variety such as a Mott gap and the mechanism of super exchange interactions. By construction, this analogue displays intertwinement of charge order with spontaneous currents and parity breaking. A novel aspect is commensurate lock-in and higher-order commensurate stability regions, when doped, which have striking similarities to the stripe phases found in cuprates. Our results suggest that these features as well as the just discussed algebraic resistivity at low temperature are representative of the new class of strongly correlated matter, characterized by strong entanglement and lack of localization and charge quantization.

Methods

Methods, including statements of data availability and any associated accession codes and references, are available at https://doi.org/10.1038/s41567-018-0217-6.

Received: 10 October 2017; Accepted: 15 June 2018;
Published online: 23 July 2018

References

1. Zaanen, J., Sawatzky, G. & Allen, J. Band gaps and electronic structure of transition-metal compounds. *Phys. Rev. Lett.* **55**, 418–421 (1985).
2. Phillips, P. Colloquium: Identifying the propagating charge modes in doped Mott insulators. *Rev. Mod. Phys.* **82**, 1719–1742 (2010).
3. Fradkin, E. *Field Theories of Condensed Matter Physics* (Cambridge Univ. Press, Cambridge, 2013).
4. Wen, X.-G. *Quantum Field Theory of Many-Body Systems: from the Origin of Sound to an Origin of Light and Electrons* (Oxford Univ. Press, Oxford, 2004).

5. Zaanen, J., Krueger, F., She, J., Sadri, D. & Mukhin, S. Pacifying the Fermi-liquid: battling the devious fermion signs. *Iran. J. Phys. Res.* **8**, 111 (2008).
6. Zaanen, J., Sun, Y.-W., Liu, Y. & Schalm, K. *Holographic Duality in Condensed Matter Physics* (Cambridge Univ. Press, Cambridge, 2015).
7. Keimer, B., Kivelson, S., Norman, M., Uchida, S. & Zaanen, J. From quantum matter to high-temperature superconductivity in copper oxides. *Nature* **518**, 179–186 (2015).
8. Fradkin, E., Kivelson, S. A. & Tranquada, J. M. Colloquium: Theory of intertwined orders in high temperature superconductors. *Rev. Mod. Phys.* **87**, 457–482 (2015).
9. Mesaros, A. et al. Commensurate $4a_0$-period charge density modulations throughout the $Bi_2Sr_2CaCu_2O_{8+x}$ pseudogap regime. *Proc. Natl Acad. Sci. USA* **113**, 12661–12666 (2016).
10. Ammon, M. & Erdmenger, J. *Gauge/Gravity Duality: Foundations and Applications* (Cambridge Univ. Press, Cambridge, 2015).
11. Faulkner, T., Iqbal, N., Liu, H., McGreevy, J. & Vegh, D. Strange metal transport realized by gauge/gravity duality. *Science* **329**, 1043–1047 (2010).
12. Iqbal, N., Liu, H. & Mezei, M. in *String Theory and Its Applications* (eds Dine, M., Banks, T. & Sachdev, S.) 707–815 (World Scientific, Singapore, 2012).
13. Policastro, G., Son, D. T. & Starinets, A. O. The shear viscosity of strongly coupled $N = 4$ supersymmetric Yang–Mills plasma. *Phys. Rev. Lett.* **87**, 081601 (2001).
14. Hartnoll, S. A., Lucas, A. & Sachdev, S. *Holographic Quantum Matter* (MIT Press, Cambridge, MA, 2018).
15. Zaanen, J. & Sawatzky, G. Systematics in band gaps and optical spectra of 3D transition metal compounds. *J. Solid State Chem.* **88**, 8–27 (1990).
16. Rozenberg, M. et al. Optical conductivity in Mott–Hubbard systems. *Phys. Rev. Lett.* **75**, 105–108 (1995).
17. Anderson, P. Antiferromagnetism. Theory of superexchange interaction. *Phys. Rev.* **79**, 350–356 (1950).
18. Zaanen, J. & Sawatzky, G. The electronic structure and superexchange interactions in transition-metal compounds. *Can. J. Phys.* **65**, 1262–1271 (1987).
19. Zaanen, J. & Gunnarsson, O. Charged magnetic domain lines and the magnetism of high-T_c oxides. *Phys. Rev. B* **40**, 7391–7394 (1989).
20. Tranquada, J., Sternlieb, B., Axe, J., Nakamura, Y. & Uchida, S. Evidence for stripe correlations of spins and holes in copper oxide superconductors. *Nature* **375**, 561–563 (1995).
21. Vojta, M. Lattice symmetry breaking in cuprate superconductors: stripes, nematics, and superconductivity. *Adv. Phys.* **58**, 699–820 (2009).
22. Zheng, B.-X. et al. Stripe order in the underdoped region of the two-dimensional Hubbard model. *Science* **358**, 1155–1160 (2017).
23. Huang, E. W. et al. Numerical evidence of fluctuating stripes in the normal state of high-T_c cuprate superconductors. *Science* **358**, 1161–1164 (2017).
24. Donos, A. & Gauntlett, J. P. Holographic charge density waves. *Phys. Rev. D* **87**, 126008 (2013).
25. Fauqué, B. et al. Magnetic order in the pseudogap phase of high-T_c superconductors. *Phys. Rev. Lett.* **96**, 197001 (2006).
26. Li, Y. et al. Unusual magnetic order in the pseudogap region of the superconductor $HgBa_2CuO_4+\delta$. *Nature* **455**, 372–375 (2008).
27. Li, Y. et al. Hidden magnetic excitation in the pseudogap phase of a high-T_c superconductor. *Nature* **468**, 283–285 (2010).
28. Zhao, L. et al. A global inversion-symmetry-broken phase inside the pseudogap region of $YBa_2Cu_3O_y$. *Nat. Phys.* **13**, 250–254 (2017).
29. Li, Q., Hücker, M., Gu, G., Tsvelik, A. & Tranquada, J. Two-dimensional superconducting fluctuations in stripe-ordered $La_{1.875}Ba_{0.125}CuO_4$. *Phys. Rev. Lett.* **99**, 067001 (2007).
30. Rajasekaran, S. et al. Probing optically silent superfluid stripes in cuprates. *Science* **359**, 575–579 (2018).
31. Hamidian, M. H. et al. Detection of a Cooper-pair density wave in $Bi_2Sr_2CaCu_2O_{8+x}$. *Nature* **532**, 343–347 (2016).
32. Ooguri, H. & Park, C.-S. Holographic end-point of spatially modulated phase transition. *Phys. Rev. D* **82**, 126001 (2010).
33. Donos, A. & Gauntlett, J. P. Holographic striped phases. *J. High Energy Phys.* **2011**, 140 (2011).
34. Cai, R.-G., Li, L., Wang, Y.-Q. & Zaanen, J. Intertwined order and holography: The case of parity breaking pair density waves. *Phys. Rev. Lett.* **119**, 181601 (2017).
35. Withers, B. Holographic checkerboards. *J. High Energy Phys.* **2014**, 102 (2014).
36. Flauger, R., Pajer, E. & Papanikolaou, S. A striped holographic superconductor. *Phys. Rev. D* **83**, 064009 (2011).
37. Liu, Y., Schalm, K., Sun, Y.-W. & Zaanen, J. Lattice potentials and fermions in holographic non Fermi-liquids: Hybridizing local quantum criticality. *J. High Energy Phys.* **2012**, 036 (2012).
38. Horowitz, G. T., Santos, J. E. & Tong, D. Optical conductivity with holographic lattices. *J. High Energy Phys.* **2012**, 168 (2012).
39. Horowitz, G. T., Santos, J. E. & Tong, D. Further evidence for lattice-induced scaling. *J. High Energy Phys.* **2012**, 102 (2012).
40. Donos, A. & Gauntlett, J. P. The thermoelectric properties of inhomogeneous holographic lattices. *J. High Energy Phys.* **2015**, 035 (2015).
41. Rangamani, M., Rozali, M. & Smyth, D. Spatial modulation and conductivities in effective holographic theories. *J. High Energy Phys.* **2015**, 024 (2015).
42. Langley, B. W., Vanacore, G. & Phillips, P. W. Absence of power-law mid-infrared conductivity in gravitational crystals. *J. High Energy Phys.* **2015**, 163 (2015).
43. Pokrovsky, V. & Talapov, A. Ground state, spectrum, and phase diagram of two-dimensional incommensurate crystals. *Phys. Rev. Lett.* **42**, 65–67 (1979).
44. Bak, P. Commensurate phases, incommensurate phases and the devil's staircase. *Rep. Progress. Phys.* **45**, 587–629 (1982).
45. Andrade, T. & Krikun, A. Commensurate lock-in in holographic non-homogeneous lattices. *J. High Energy Phys.* **2017**, 168 (2017).
46. Braun, O. & Kivshar, Y. *The Frenkel–Kontorova Model: Concepts, Methods and Applications* (Springer, Berlin, Heidelberg, 2004).
47. Comin, R. & Damascelli, A. Resonant x-ray scattering studies of charge order in cuprates. *Annu. Rev. Condens. Matter Phys.* **7**, 369–405 (2016).
48. Boebinger, G. et al. Insulator-to-metal crossover in the normal state of $La_{2-x}Sr_xCuO_4$ near optimum doping. *Phys. Rev. Lett.* **77**, 5417–5420 (1996).
49. Laliberte, F. et al. Origin of the metal-to-insulator crossover in cuprate superconductors. Preprint at http://arXiv.org/abs/1606.04491 (2016).
50. Grozdanov, S., Lucas, A., Sachdev, S. & Schalm, K. Absence of disorder-driven metal-insulator transitions in simple holographic models. *Phys. Rev. Lett.* **115**, 221601 (2015).
51. Donos, A., Goutéraux, B. & Kiritsis, E. Holographic metals and insulators with helical symmetry. *J. High Energy Phys.* **2014**, 038 (2014).
52. Donos, A. & Hartnoll, S. A. Interaction-driven localization in holography. *Nat. Phys.* **9**, 649–655 (2013).
53. Donos, A. & Gauntlett, J. P. Novel metals and insulators from holography. *J. High Energy Phys.* **2014**, 007 (2014).
54. Goutéraux, B. Charge transport in holography with momentum dissipation. *J. High Energy Phys.* **2014**, 181 (2014).

Acknowledgements

We thank J. Gauntlett, A. Donos, B. Gouteraux, N. Kaplis, C. Pantelidou and J. Santos for insightful discussions. The research of K.S., A.K. and J.Z. was supported in part by a VICI (K.S.) award of the Netherlands Organization for Scientific Research (NWO), by the Netherlands Organization for Scientific Research/Ministry of Science and Education (NWO/OCW) and by the Foundation for Research into Fundamental Matter (FOM). The work of T.A. is supported by the ERC Advanced Grant GravBHs-692951. He also acknowledges the partial support of the Newton–Picarte grant 20140053. Numerical calculations have been performed on the Maris Cluster of the Lorentz Institute.

Author contributions

The numerical work and the analysis was carried out in close collaboration between A.K. and T.A. In the conception of the project K.S. and J.Z. played a key role, and J.Z. helped to guide the research resting on his condensed-matter expertise while K.S. added his field theoretical and holographic duality know-how. The manuscript was written jointly by all authors while A.K. is responsible for the figures.

Competing interests

The authors declare no competing interests.

Additional information

Supplementary information is available for this paper at https://doi.org/10.1038/s41567-018-0217-6.

Reprints and permissions information is available at www.nature.com/reprints.

Correspondence and requests for materials should be addressed to A.K.

Publisher's note: Springer Nature remains neutral with regard to jurisdictional claims in published maps and institutional affiliations.

Methods

The holographic set-up. We consider the model of ref. [33] that consists of 3+1-dimensional Einstein–Maxwell theory coupled to a neutral pseudo scalar. Following refs [55,56], we write the action as

$$\begin{aligned} S &= \int \mathrm{d}^4x\sqrt{-g}\left(R-\frac{1}{2}(\partial\psi)^2-\frac{\tau(\psi)}{4}F^2-V(\psi)\right) \\ &\quad -\frac{1}{2}\int \vartheta(\psi)F\wedge F+S_{bndy} \end{aligned} \tag{2}$$

where

$$S_{bndy}=-\int \mathrm{d}^3x\sqrt{-h}\,(K-4+\psi^2) \tag{3}$$

Here $F=\mathrm{d}\mathcal{A}$ is the field strength associated with the Maxwell field $\mathcal{A}$, while h is the metric induced at the boundary with extrinsic curvature K. The boundary term (2) obtained in ref. [56] renormalizes the action[57]. Following refs [33,55,56,58], we choose the couplings as

$$\begin{aligned} V(\psi) &\equiv 2\Lambda+W(\psi)=-6\cosh(\psi/\sqrt{3}), \\ \tau(\psi) &= \frac{1}{\cosh(\sqrt{3}\psi)}, \\ \vartheta(\psi) &= \frac{c_1}{6\sqrt{2}}\tanh(\sqrt{3}\psi) \end{aligned} \tag{4}$$

This model is bottom-up, but similar couplings can be obtained in supergravity[59]. The cosmological constant is $\Lambda=-3$ and the mass of the scalar is $m^2=-2$. The equations of motion admit the translational invariant Reissner–Nordström charged black hole solution

$$\begin{aligned} \mathrm{d}s^2 &= \frac{1}{z^2}\left(-f(z)\mathrm{d}t^2+\frac{\mathrm{d}z^2}{f(z)}+\mathrm{d}x^2+\mathrm{d}y^2\right), \\ A &= \overline{\mu}\,(1-z)\mathrm{d}t, \\ \psi &= 0 \end{aligned} \tag{5}$$

where

$$f=(1-z)(1+z+z^2-\overline{\mu}^2z^3/4) \tag{6}$$

with the boundary at $z=0$ and the horizon at $z=1$. The chemical potential in the dual theory is given by the constant $\overline{\mu}$. The Hawking temperature reads

$$\overline{T}=\frac{12-\overline{\mu}^2}{16\pi} \tag{7}$$

We are interested in stationary configurations of the form

$$\mathrm{d}s^2=\frac{1}{z^2}\left(-Q_{tt}f(z)\mathrm{d}t^2+Q_{zz}\frac{\mathrm{d}z^2}{f(z)}+Q_{xx}(\mathrm{d}x+Q_{zx}\mathrm{d}z)^2+Q_{yy}(\mathrm{d}y+Q_{ty}\mathrm{d}t)^2\right) \tag{8}$$

$$\mathcal{A}=A_t\mathrm{d}t+A_y\mathrm{d}y \tag{9}$$

All unknowns are functions of z and the boundary coordinate x. We search for black holes with uniform temperature, which means that in the near horizon all functions must be regular except $f(z)$. Then, the equations of motion require $Q_{tt}(1,x)=Q_{zz}(1,x)$, which implies that the surface gravity is constant and given by equation (7) (see, for example, ref. [38]). Given that the dual field theory lives in flat space, we require the metric to be asymptotically AdS as $z\to 0$. The AdS/CFT dictionary[60–62] relates the boundary asymptotics of the fields in equation (2) to the sources and one-point functions of the energy-momentum tensor, electromagnetic currents and parity-odd order parameter in the dual 2+1-dimensional theory. In particular, from the ultraviolet expansions

$$Q_{tt}=1+z^2Q_{tt}^{(2)}(x)+z^3Q_{tt}^{(3)}(x)+O(z^4) \tag{10}$$

$$A_t=\mu(x)-z\rho(x)+O(z^2) \tag{11}$$

$$A_y=zJ_y(x)+O(z^2) \tag{12}$$

$$\psi=z^2\psi^{(2)}(x)+O(z^3) \tag{13}$$

we obtain that the coefficients $\mu(x)$, $\rho(x)$, $J_y(x)$ and $\psi^{(2)}(x)$ determine the chemical potential, charge density, current density and pseudoscalar parity-breaking order parameter of the dual theory and the energy density is given by

$$\epsilon(x)=2+\frac{\overline{\mu}^2}{2}-3Q_{tt}^{(3)}(x) \tag{14}$$

To break translations explicitly, we introduce a spatially modulated chemical potential[36,39], fixing $A_t(z=0,x)=\mu(x)$ with

$$\mu(x)=\mu_0(1+A\cos(\overline{k}\,x)) \tag{15}$$

Without loss of generality, we set $\mu_0=\overline{\mu}$ (ref. [63]). We express the dimensionful parameters of the model in units of $\overline{\mu}$:

$$\overline{T}=T\overline{\mu}\,,\quad \overline{k}=k\overline{\mu}\,,\quad \overline{p}=p\overline{\mu} \tag{16}$$

When $\psi=Q_{ty}=A_y=0$, all profiles acquire modulation along x solely due to the x-dependent boundary conditions, so these solutions represent states that break translations only explicitly—'ionic lattices'[39]. For small ω, the optical conductivity can be approximated by a Drude peak with a finite d.c. value. These lattices are irrelevant in the infrared, in the sense that the near-horizon geometry approaches the translationally invariant charged black hole as the temperature goes to zero[40]. As a result of this, one can think of the lattice as an ultraviolet-based structure (see Fig. 2).

For translations to be broken only spontaneously, the boundary conditions need to be translational invariant in the ultraviolet, so we take $A=0$ in equation (15), along with the vanishing of leading terms in A_y and ψ, as reflected by equations (10)–(13) (see also refs [55,56,58,63]).

In the case of purely spontaneous symmetry breaking, all of the boundary sources can be made homogeneous: $A=0$ in equation (15)[55,56,58,63]. However, the spatial modulation arises dynamically as an infrared effect, due to near-horizon instabilities induced by the ϑ-term in equation (2). The effect localizes near the horizon of the black hole as seen in Fig. 2. The resulting spontaneous structure is strongly dependent on $\overline{\mu}\neq 0$ and the value of the coupling c_1 in equation (4): increasing c_1 raises the critical temperature and makes the spontaneous crystal more stable, leading to more pronounced commensurate effects. For this reason, we choose $c_1=17$, as opposed to refs [33,55,56,58].

The arising spontaneous structure is characterized by the oscillating values of A_y and ψ, which results in the observable staggered currents $J_y(x)$. At the nonlinear level, A_t also becomes modulated with twice the momentum of A_y or ψ due to the quadratic interaction in the ϑ-term (equation (1)) (see Supplementary Fig. 3b). The modulation of A_t corresponds to the formation of a CDW on the boundary, which we write as

$$\rho_{CDW}\approx\rho_0+\delta\rho\cos(\overline{p}\,x) \tag{17}$$

We use the momentum of this CDW $\overline{p}$ as the defining momentum to describe the spontaneous structure; that is, the staggered currents have momentum $\overline{p}/2$. This notation differs from previous studies[33,45,55,56,58]. To compare the results, we note $p_{\mathrm{here}}=2p_{\mathrm{there}}$.

It is instructive to first consider spontaneous symmetry perturbatively by taking ψ, A_y and Q_{ty} to be linearly small in a Fourier basis of momentum p and zero frequency. Linear instabilities exist for $T<T_c$ and arrange themselves in a bell-shaped curve in the (T,p) plane[33], as in the five-dimensional case[64] (see Supplementary Fig. 1a). The critical temperature in purely spontaneous case of Reissner-Nordström background corresponds to the maximum of the bell $T_c^{RN}=0.147$, attained at a critical momentum $p_c^{RN}=1.33$. Inside the bell curve, one can construct nonlinear solutions for a range of values of p. However, the ones that minimize the (spatially averaged) thermodynamic potential play a special role since they dominate the thermodynamic ensemble. These preferred solutions for all T form a line $p_0(T)$ inside the bell curve, which in general deviates from p_c^{RN}.

We can study the interplay of the explicit and spontaneous symmetry-breaking phenomena in two ways: we can start with an ionic lattice and observe how the instabilities towards the formation of spontaneous structures develop, or begin with a configuration that breaks translations of the Reissner–Nordström solution spontaneously and introduce a modulated source as in equation (15). Following the former procedure, we examine the unstable modes of the pure ionic lattice solution. The study of these modes was undertaken in an earlier study[45], which revealed an interesting lock-in pattern of the spontaneous to the explicit structure. We reproduced the calculations of ref. [45] for the parameters that will be used in our nonlinear study: $A=0.7$ and $c_1=17$ (see Supplementary Fig. 1b,c). We observe the lock-in of the spontaneous structure indicated by the plateaux at $p_c/k=1$ and $p_c/k=2$. Importantly, the higher-order commensurate fractions (that is, $p_c/k=3/2$) cannot be observed in the perturbative approach. When the spontaneous structure is infinitesimal, the total solution including the perturbative modes is forced by the lattice to be periodic with momentum k. Hence, near critical temperature all possible commensurate fractions of p_c/k are integers. This changes when one considers finite amplitude of the spontaneous structure; the result is Fig. 3a.

Full back-reacted solutions. We construct the fully back-reacted solutions by observing how a given purely spontaneous structure arising from the

Reissner–Nordström background gets modified as we introduce an ionic lattice potential by increasing the amplitude from $A=0$.

We wish to study the thermodynamic stability of these configurations, by minimizing the spatially averaged thermodynamic potential

$$\Omega(x)=\epsilon(x)-\overline{T}s(x)-\mu(x)\rho(x) \tag{18}$$

where ϵ is the energy density, $\overline{T}$ is the temperature, s is the entropy density, μ is the x-dependent chemical potential and ρ is the charge density.

There is a technical difficulty, which arises while addressing the nonlinear solutions. This involves two unrelated length scales: the wavelength of the spontaneous structure $\lambda_p=2\pi/p$ and the wavelength of the background lattice $\lambda_k=2\pi/k$. To set up the numerical PDE solver, one has to specify only one scale, corresponding to the size of the computational domain with periodic boundary conditions. Therefore, in practice we can access only the values λ_p that are rational multiples of λ_k:

$$\lambda_p=\frac{N_k}{N_p}\lambda_k, \quad N_k,N_p\in\mathbb{N} \tag{19}$$

In this case, one can choose the computation domain of size $N_k\lambda_k$ equal to the integer number of lattice periods, which would simultaneously accommodate N_p periods of CDW. This situation is analogous to the 'magnetic unit cell' phenomenon, which arises when one considers a crystal in an external magnetic field. The unit cell must simultaneously accommodate the integer number of crystal plaquettes and magnetic fluxes, and can become substantially large[65]. We see here that the accessible range of spontaneous structure wavevectors k is now discrete and its density is limited by the maximal size of the computational domain, which we can handle in our numerics. In what follows, we will use computational domains including up to $N_k=20$ periods of the lattice or up to $N_p=20$ periods of the spontaneous CDW (note, once again, that this corresponds to 10 periods in the spontaneous currents), which allows us to achieve reasonable resolution of the corresponding thermodynamic potentials (see Supplementary Fig. 2).

In practice, to construct the solution with N_p CDW periods on top of the N_k lattice cells with period λ_k and amplitude A, we first find the spontaneous stripe solution with specific period λ_p from equation (19) on top of the translationally symmetric background. Then we concatenate N_p copies of these stripes fitting them in the enlarged calculation domain. At this point, we turn on N_k periods of the background lattice by slowly changing the boundary condition for the chemical potential, eventually achieving the desired value of A in equation (15). This adiabatic process preserves the initial number of CDW periods that we check numerically at every stage by counting the number of zeros of the oscillating A_y field at the horizon (see Supplementary Fig. 3c,d).

We explore the phase diagram at a given temperature by first choosing the period and the amplitude of the explicit ionic lattice. Then we construct a set of nonlinear solutions, corresponding to the spontaneous structures with different wavevectors p on top of this lattice. We calculate the thermodynamic potential (18) for these solutions and find the thermodynamically preferred one. The sample of the $\Omega(k)$ curves is shown in Supplementary Fig. 2.

A good check of our calculation is that, at $A=0$ our solutions follow the curve, which one would obtain in the study of the spontaneous striped solutions on the homogeneous Reissner–Nordström background[55,56,58]. We have checked that for $c_1=9.9$ our results coincide with Fig. 2 in ref. [55]. Even though we have access only to the discrete set of values, they lie on smooth curves that have well-defined minima. One interesting feature of these curves is that they end abruptly for $N_p/N_k<1$. This can be understood via a simple energy argument. In the present case where $p_0>k$, the solutions with $N_p/N_k>1$ are stabilized by the competition between the lattice commensuration and the elasticity of the spontaneous structure. In the case of $N_p/N_k<1$, both of these effects tend to destroy the state; therefore, it is dynamically unstable and we do not obtain the corresponding solutions as local minima of the free energy (see ref. [66] for more details).

One can see that as the amplitude rises, the minimum smoothly shifts from the incommensurate to commensurate point. Thus, by increasing the amplitude, we observe the smooth, at least second-order phase transition. The different commensurate points, which are thermodynamically stable at different temperatures and charge densities, are shown in Fig. 3a.

Commensurate state. Let us first focus on two integer-value commensurate states: the leading 1/1 Mott insulator and the higher 2/1 commensurate state. The features of the 1/1 state (Supplementary Fig. 3a) are mostly similar to those of the pure spontaneous crystal with an important difference: now the periodicity of the overall structure is anchored by the ionic lattice wavelength λ_k. The staggered currents are seen, but they are now enhanced near the maxima of $\rho(x)$ and suppressed at the minima. This leads to the effective localization of the currents. On the other hand, the spontaneous structure brings an excess of total charge density as compared to the pure lattice (shaded region in Supplementary Fig. 3a, colour in Fig. 1a–d). This allows us to define a 'unit of CDW charge', q_{CDW} (equation (20)) as the integrated excess charge density in the unit cell

$$q_{\mathrm{CDW}}\equiv\frac{k}{2\pi}\int_0^{2\pi/k}(\rho_{Mott}(x)-\rho_{lattice}(x)) \tag{20}$$

An important feature is that in holography q_{CDW} assumes a continuous range of values depending on the external conditions, while in the hard Mott insulator it would be quantized in units of the electron charge.

Now we address the higher commensurate state 2/1 (see Supplementary Fig. 3b). Note that the localized peaks of the J_y current are all aligned. The reason is that the 2/1 commensurate state has twice the number of CDW periods as compared to the 1/1 state (see the near-horizon profile in Supplementary Fig. 3c,d). Every odd positive current peak is thus enhanced by the charge density, but the negative currents are dispersed and do not show well-defined peaks. Nonetheless, the total current remains zero. Supplementary Fig. 8b shows that the total charge density of this 'aligned' state is larger than that of the staggered one. This is due to the fact that it possess twice the number of spontaneous CDWs per unit cell, each bringing contributions of order q_{CDW} to the total charge density. This feature allows us to denote this state as 100% doped and define the doping rate as in the main text.

Incommensurate state. As we mentioned earlier, the numerical computation in the incommensurate state is technically more involved, as the numbers of periods in equation (19) become large. The isolated discommensuration is found as a solution that is closest to the commensurate $\frac{N_p}{N_k}=\frac{1}{1}$ value. Given that

$$\left|\frac{N_p}{N_k}-\frac{1}{1}\right|=\frac{|N_p-N_k|}{N_k} \tag{21}$$

we will choose $N_k=N_p-1$ and maximal N_p reachable by our numerics $N_p\leq 20$. The incommensurate solution with 20 CDWs per 19 lattice periods would have exactly one excess CDW period per 19 unit cells as compared to the commensurate state. Inspecting this solution (Fig. 4), we see that the solution profile coincides with the commensurate state almost everywhere except from the finite size region in the core, where this excess of one period of CDW is accounted for. We can also study the thermodynamic potential and charge density of this solution as compared to the pure commensurate state (Supplementary Fig. 4), which shows that this incommensurate solution can be seen as a commensurate state with one localized soliton on top of it. This soliton is a direct analogue of discommensuration studied in the context of CDWs in previous studies[43,67].

As is apparent in Supplementary Fig. 4, a single discommensuration possesses a finite net charge

$$q_{\mathrm{disc.}}=\frac{1}{19\lambda_k}\int_0^{19\lambda_k}\rho_{20/19}(x)-\rho_{1/1}(x)\mathrm{d}x \tag{22}$$

which is manifestly positive, is of order q_{CDW} (equation (20)) and has a direct analogue in the hard Mott insulator model. Indeed, the discommensurations in the conventional Mott state are associated with one extra or missing electron in the unit cell. In this case, the charge of the discommensuration would be exactly 1. The holographic model, in contrast, allows for continuous variations in $q_{\mathrm{disc.}}$ (see Fig. 3c).

One can see that further deviation from the commensurate point 1/1, according to equation (21), is achieved by raising the density of discommensurations. At higher commensurate points they can form a super lattice with a period of several ionic lattice constants a (Fig. 4c). For instance, the discommensuration lattice with $3a$ period corresponds to the commensurate fraction $p/k=N_p/N_k=4/3$, which is stable at low temperature in a window of doping levels as shown on the phase diagram Fig. 3a.

Optical conductivity. To further investigate the properties of the above-described solutions, we extract their electric conductivity as a function of frequency, $\sigma(\omega)$, along the x direction, following ref. [41]. The optical conductivity in inhomogeneous set-ups has also been studied in, for example, refs [38–40].

Extracting $\sigma(\omega)$ is an involved numerical problem, which requires one to first construct a given background to sufficient accuracy and then solve the perturbation equations on top of this solution. We found that our usage of the standard `MachinePrecision` computations of Wolfram Mathematica[68] limits the reliability of our a.c. conductivity results to the region in the vicinity of the critical temperature. For the results within this region, we successfully perform a set of numerical consistency checks, which includes vanishing of the constrains and gauge fixing conditions. We have also checked that our results satisfy the sum rule on the integrated spectral weight: $\lim_{\omega\to 0}S(\omega)\to 0$, where

$$S(\omega/\mu)\equiv\int_0^{\omega/\mu}(\Re\,[\sigma(\omega')]-1)\,\mathrm{d}\omega' \tag{23}$$

If one is interested only in the d.c. conductivity, $\sigma_{\mathrm{d.c.}}=\sigma(\omega=0)$, it is possible to largely simplify the calculation since we can obtain a formula for this observable solely in terms of the horizon data[40,69–72]. The relevant formula for our system was obtained in ref. [72], which we have rederived in full agreement. Moreover, for all of the cases we have studied, the limit $\omega\to 0^{+}$ of $\sigma(\omega)$ agrees with the computation of $\sigma_{\mathrm{d.c.}}$ in terms of the horizon data, which serves as another test of our numerics.

Numerical techniques and precision control. In the present study, we rely heavily on numerical analysis of nonlinear solutions. Moreover, to study the phase diagram and cover the parameter space, we have to obtain several thousand solutions, some of them requiring large calculation grids in the spatial direction. This situation places strict requirements on the numerical techniques that we use, the precision and the accuracy of the results.

We have chosen a single-patch pseudospectral scheme in the holographic direction and used Wolfram Mathematica[68] to implement the numerical algorithm. The main limitation we encounter is the necessity to work with `MachinePrecision` numbers in the compiled function, which eventually limits the precision of our results. Element-wise operations can be efficiently compiled with `Compile`, which brings up a spectacular acceleration. We use precompiled linear algebra solvers and sparse matrices, which delivers a decent speed of calculations.

It should be noted that direct inversion (Newton–Raphson method) for the case of pseudospectral discretization is extremely demanding for large grids, so we used a relaxation scheme instead. We employ the differential operator evaluated in the low-order finite-difference derivative scheme as a preconditioner. The result is a nonlinear Richardson relaxation with Orszag preconditioning (see section 15.14 and equation (15.115) in ref. [73]). Our calculation scheme takes about half an hour to obtain the precise solution on our largest grid of size $\sim 330_x\times 80_z$ (pseudospectral) using a single core of a laptop CPU (Intel Core i7-5600U at 2.60 GHz) and about 3 Gb of RAM.

As one can see from our results, the difference between the free energies of the solution with spontaneous structure and the one without is a few per cent of the free energies themselves. This means that to reliably study this difference, we need to evaluate the free energies with an accuracy of at least 10^{-4}. We observe that for a single-patch Chebyshev grid the maximum N_y resolution is limited by the rounding errors at $N_y=80$. The accuracy of the thermodynamical potential for a grid of this size is about 10^{-7}. We used this value as a numerical error estimate throughout the present study and it has proved to be sufficient to obtain our main results. One should keep in mind that in the numerical procedure we solve the modified DeTurck equations. Thus, it must be checked that the Einstein equations are satisfied, which we do by two independent measures: the maximal value of the trace of the Einstein equations and the maximum value of the norm of a DeTurck vector. For temperatures $T>0.01$, these values are both of order 10^{-7}, which is quite satisfactory[40].

Data availability. The data that support the plots within this paper and other findings of this study are available from the corresponding author upon reasonable request.

References

55. Withers, B. The moduli space of striped black branes. Preprint at http://arXiv.org/abs/1304.2011 (2013).
56. Withers, B. Black branes dual to striped phases. *Class. Quant. Grav.* **30**, 155025 (2013).
57. de Haro, S., Solodukhin, S. N. & Skenderis, K. Holographic reconstruction of space-time and renormalization in the AdS/CFT correspondence. *Commun. Math. Phys.* **217**, 595–622 (2001).
58. Donos, A. Striped phases from holography. *J. High Energy Phys.* **2013**, 059 (2013).
59. Gauntlett, J. P., Sonner, J. & Wiseman, T. Quantum criticality and holographic superconductors in M-theory. *J. High Energy Phys.* **2010**, 060 (2010).
60. Maldacena, J. M. The large *n* limit of superconformal field theories and supergravity. *Int. J. Theor. Phys.* **38**, 1113–1133 (1999).
61. Witten, E. Anti-de sitter space and holography. *Adv. Theor. Math. Phys.* **2**, 253–291 (1998).
62. Gubser, S. S., Klebanov, I. R. & Polyakov, A. M. Gauge theory correlators from noncritical string theory. *Phys. Lett. B* **428**, 105–114 (1998).
63. Rozali, M., Smyth, D., Sorkin, E. & Stang, J. B. Holographic stripes. *Phys. Rev. Lett.* **110**, 201603 (2013).
64. Nakamura, S., Ooguri, H. & Park, C.-S. Gravity dual of spatially modulated phase. *Phys. Rev. D* **81**, 044018 (2010).
65. Lifshitz, E. M. & Pitaevskii, L. P. *Statistical Physics: Theory of the Condensed State* Vol. 9 (Elsevier, Amsterdam, 2013).
66. Krikun, A. Holographic discommensurations. Preprint at http://arXiv.org/abs/1710.05801 (2017).
67. McMillan, W. Theory of discommensurations and the commensurate–incommensurate charge-density-wave phase transition. *Phys. Rev. B* **14**, 1496–1502 (1976).
68. Mathematica v10.2 (Wolfram Research, Inc., 2015).
69. Donos, A. & Gauntlett, J. P. Navier–Stokes equations on black hole horizons and DC thermoelectric conductivity. *Phys. Rev. D* **92**, 121901 (2015).
70. Banks, E., Donos, A. & Gauntlett, J. P. Thermoelectric DC conductivities and Stokes flows on black hole horizons. *J. High Energy Phys.* **2015**, 103 (2015).
71. Donos, A., Gauntlett, J. P., Griffin, T. & Melgar, L. DC conductivity of magnetised holographic matter. *J. High Energy Phys.* **2016**, 113 (2016).
72. Donos, A., Gauntlett, J. P., Griffin, T., Lohitsiri, N. & Melgar, L. Holographic DC conductivity and Onsager relations. *J. High Energy Phys.* **2017**, 006 (2017).
73. Boyd, J. P. *Chebyshev and Fourier Spectral Methods* (Courier Corporation, Chicago, 2001).